IEEE Access
Multidisciplinary | Rapid Review | Open Access Journal

Received December 31, 2019, accepted January 21, 2020, date of current version February 17, 2020.

Digital Object Identifier 10.1109/ACCESS.2020.2969274

SPPs-Shared Dual-Band Antenna With Large Frequency Ratio

JIAN-XIN CHEN[1,2], (Senior Member, IEEE), SHUAI-HUA CAO[1], AND XUE-FENG ZHANG[1,2]
[1]School of Information Science and Technology, Nantong University, Nantong 226019, China
[2]Nantong Research Institute for Advanced Communication Technologies, Nantong University, Nantong 226019, China

Corresponding author: Xue-Feng Zhang (xefeng@hotmail.com)

This work was supported in part by the Industrial Key Technologies Program of Nantong under GY22016015, in part by the Natural Science Foundation of Jiangsu Province under Grant BK20161281, and in part by the Science-Technology Programs of Nantong under Grant MS12018004.

ABSTRACT The operating frequency of future communication systems will cover both microwave and millimeter-wave (MMW) bands simultaneously. This paper presents a novel design of spoof surface plasmon polaritons (SPPs) structure-shared dual-band antenna with large frequency ratio, which consists of a planar open sleeve monopole antenna operating at S-band and a taper slot antenna (TSA) at K/Ka-band. In this design, the SPPs structure takes important roles in two aspects: it serves as an equivalent-lens to enhance the gain of TSA and a monopole of the planar open sleeve antenna to keep a low profile. To realize high isolation between the two antennas, a substrate integrated waveguide (SIW) and an integrated coaxial line are designed to feed the TSA and the planar open sleeve monopole antenna respectively. The SPPs-shared antenna shows an enhanced endfire gain of 13.09 dBi in the frequency range of 19.32-32.90 GHz and an omnidirectional gain of 1.06-2.92 dBi over the range of 2.23-3.69 GHz, keeping a compact size. The large frequency ratio of 10.8, low profile and the wide operating bands in both lower and upper frequency ranges can meet many wireless communication applications. Reasonable agreement between the measured and simulated results is observed.

INDEX TERMS Surface plasmon polaritons (SPPs), dual-band antenna, large frequency ratio, wideband antenna, planar monopole antenna, low profile, high isolation.

I. INTRODUCTION

In the future communication applications, antenna systems operating in both microwave band and millimeter-wave (MMW) band are required to increase data exchange capability [1]. One notable scenario is the design of a dual-band antenna, covering both the 2.4 GHz and 24 GHz industrial scientific medical (ISM) bands [2]. Another one is applied for the wideband communication systems, which complies with both Wi-Fi channels and wireless gigabit (WiGig) channels for future wireless local area network (WLAN) applications [3]. Nevertheless, a single multimode-resonance antenna can hardly support the microwave and MMW bands simultaneously since its frequency ratio is usually less than three [4], [5].

For the large frequency ratio case, it is a straightforward way to combine two separate antennas together. In line with this concept, many aperture-shared antennas with large frequency ratio were implemented, where the microwave and MMW parts are individually designed and then combined together either horizontally [6], [7] or vertically [8], [9]. To improve the channel isolation, the adequate distance between the antennas is necessary, leading to low aperture efficiency and uncompact structure. For most practical applications, the compact and low profile antennas are more attractive.

Recently, many structure-shared approaches have been proposed for compact purpose [10]–[12]. For instance, a dielectric resonator (DR) and a MMW Fabry-Perot resonator are combined in [13], [14] by sharing a dielectric block to realize a dual-band antenna. The antenna in [15] shows a lower profile than the common DR antenna (DRA) and a high aperture efficiency is achieved by reusing a substrate integrated waveguide (SIW) cavity as a patch antenna at low frequency.

In the MMW band, the path loss becomes prominent when the electromagnetic (EM) wave travels in free space, leading to a short transmission distance [16]. To overcome this issue, high-gain antennas along with the wide bandwidth (BW) are highly desired to compensate for the propagation loss

The associate editor coordinating the review of this manuscript and approving it for publication was Giovanni Angiulli.

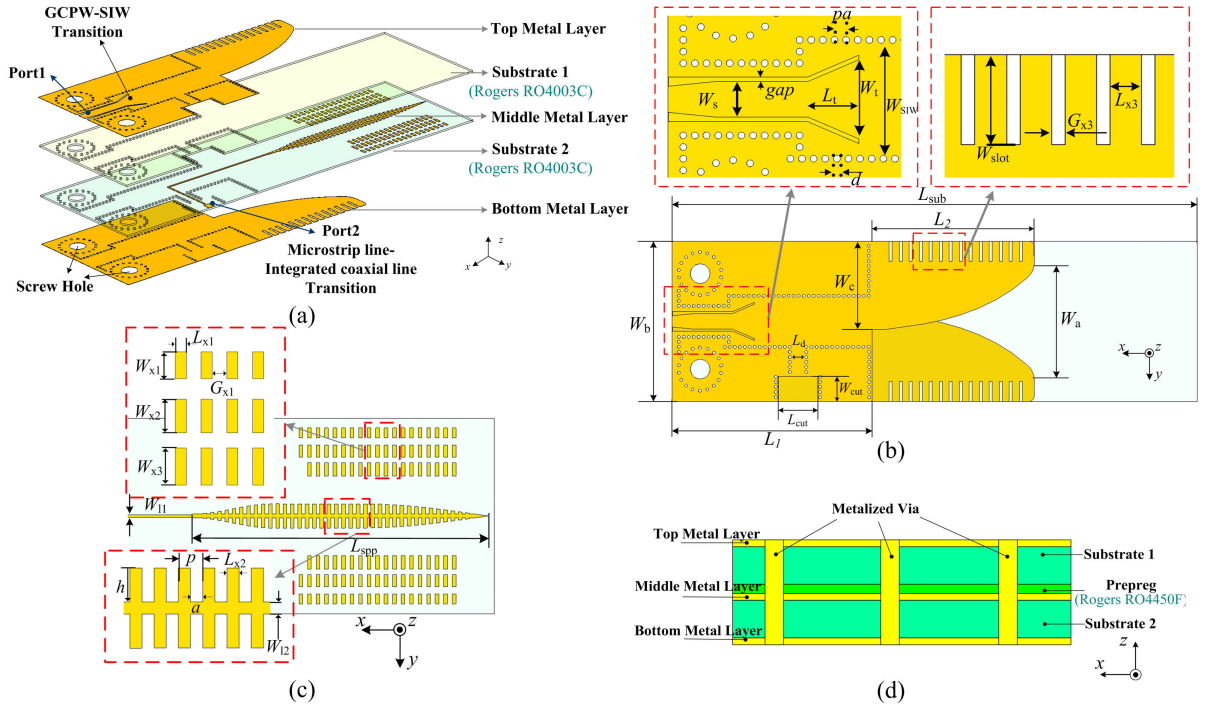

Parameters of optimized antenna

Parameters	L_{sub}	W_b	L_l	L_2	L_d	W_{cut}	L_{cut}	W_a	d	W_{l1}	W_{l2}	W_{x1}	W_{x2}	W_{x3}	h	G_{x1}	W_c
Value(mm)	52.5	16	20	16.2	2.16	2.5	4	11.74	0.3	0.2	0.3	0.8	1	1.1	0.85	0.4	8.8
Parameters	W_s	gap	L_t	W_t	W_{SIW}	pa	L_{spp}	p	a	G_{x3}	L_{x1}	L_{x2}	L_{x3}	W_{slot}	A	B	
Value(mm)	1.52	0.2	2.2	3.4	4.8	0.5	24.35	0.6	0.3	0.3	0.3	0.3	0.7	2	0.7	0.15	

FIGURE 1. Geometry of the proposed dual-band antenna. (a) 3-D view. (b) Top and bottom metal layer. (c) Middle metal layer. (d) Cross view of the proposed antenna (not to scale).

and to increase the channel capability. Antenna arrays are commonly utilized to produce high gain [17]–[19]. But the feeding network complicates antenna designs and also causes extra loss, reducing antenna efficiency. Dielectric lens antennas show a high directivity and BW [20], [21], but they generally suffer from the bulky volume, heavy weight, and expensive fabrication costs. In recent years, metamaterial and metasurface (2D case of the metamaterial) have become an appealing subject of research because of their exotic properties. They have been explored in many antenna applications, such as holographic antennas [22], [23], metasurface planar lenses [24]–[26], and metasurface superstrate [27], [28]. Most recently, the surface plasmon polaritons (SPPs) structure has been implemented to adjust EM wave propagation since the EM wave propagating in the structure shows slow wave feature [29].

In this paper, a novel SPPs-shared technique is proposed. Different with [29], the SPPs structure serves as not only the metasurface lens in the MMW band, but also as the radiator of the planar sleeve antenna working in the microwave band. The orthogonal transverse electromagnetic (TEM) mode and transverse electric (TE) mode, guiding in the integrated coaxial cable and SIW respectively, are employed to obtain high isolation between the microwave and MMW signals. The low profile, compact size, wideband and high gain, shown by the proposed antenna, are appealing to the applications in wireless communication systems.

II. ANTENNA DESIGN

Fig. 1(a) shows the proposed dual-band antenna with multilayer dielectric substrates. The top (Substrate 1) and bottom (substrate 2) Rogers RO4003C substrates with dielectric constant of 3.55 and tangent loss of 0.0027, each with the same thickness of 0.2 mm, are bonded with a 0.1 mm thick Rogers 4450F prepreg (dielectric constant of 3.7 and tangent loss of 0.004). Two metal layers patterned on the top and bottom surfaces of the multilayer substrate form a SIW-fed taper slot antenna (TSA). The detailed structure of the TSA is shown in Fig. 1(b), where two flared arms are combined to form an exponentially tapered slot between the top and bottom metal sheets. The edge curves of the flared arms are determined by the equation $y = Ae^{Bx}$ with the coefficients of A and B. To enhance the gain of the TSA, a composite metasurface consisting of a corrugated SPPs structure and the coplanar metal grid arrays is patterned on middle layer to form a metasurface lens, as shown in Fig. 1(a). The enlarged schematic of the meatasurface is shown in Fig. 1(c). The SPPs structure and the flared arms of the TSA are shared as

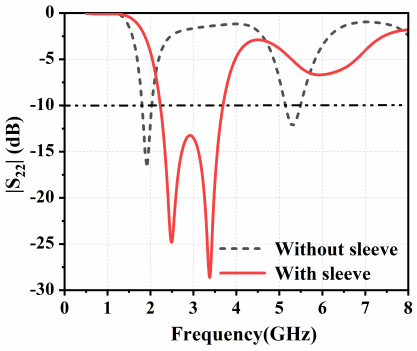

FIGURE 2. Comparison of the reflection coefficients between the antennas with and without parasitic flared arms (sleeve).

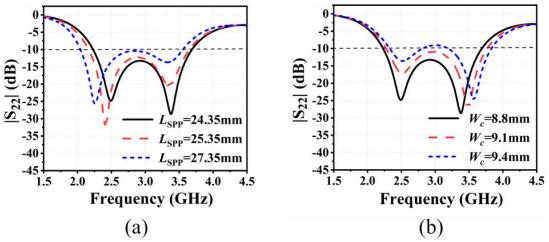

FIGURE 3. Simulated reflection coefficients of the sleeve monopole antenna with different (a) total lengths of the SPPs structure (L_{spp}) and (b) widths of parasitic units (W_c).

a monopole and parasitic radiators by a planar open sleeve antenna operating at a lower frequency band. The integrated coaxial line (TEM mode) and the SIW (TE mode) are used to feed the sleeve monopole antenna and the TSA respectively to achieve high isolation. All the metalized via holes are drilled throughout all layers as shown in Fig. 1(d). The specific parameters of the dual-band antenna are indicated in Fig. 1(b) and (c), and their values are tabulated at the bottom of Fig. 1. The dimensions of the proposed dual-band antenna are $52.5\times16\times0.51\text{mm}^3$, showing a compact size and a low profile of the antenna.

A. CO-DESIGN OF THE SPPs-SHARED DUAL-BAND ANTENNA

The shared SPPs structure plays an important role both in the TSA and the sleeve monopole antenna. For the TSA, a longer SPPs strip is favorable to enhance its gain. However, the length of the SPPs strip (L_{spp}) also determines the working frequency (the first resonance frequency shown in Fig. 2) of the omnidirectional sleeve monopole antenna [30]. Therefore, the length L_{spp} is primarily chosen as a quarter wavelength of EM wave at 2 GHz and finely tuned according the parametric study shown in Fig. 3(a). The corrugations on the SPPs strip can be safely neglected at the microwave S-band, i.e. the strip can be treated as a smooth metal strip, because the depth of the corrugations is much less than the operating wavelength.

The two flared arms of the TSA are shared by the sleeve monopole antenna as parasitic radiators to broaden the BW by introducing the second resonance as shown in Fig. 2.

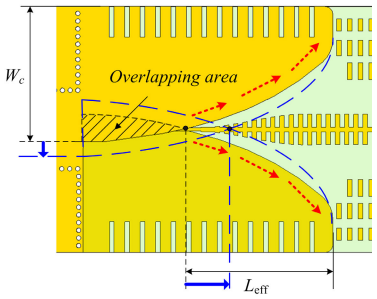

FIGURE 4. Variation of the current path on the sleeve (L_{eff}) with width of the flared arms (W_c). The current (dotted red line) on the parasitic sleeve unit at the second resonance frequency.

When the length of the flared arm is preliminarily chosen according to the gain and operating band of the TSA, the effective lengths (L_{eff}) of the parasitic arms can be tuned by their widths (W_c), as schematically shown in Fig. 4. The overlap between the arms enlarges with increasing W_c, thus shortening the current path on the arms. The decrease of L_{eff} leads to the second resonance frequency shifts to upper frequency, which manifests as the increase of frequency with W_c, as depicted in Fig. 3(b). The value of W_c is finally set to 8.8 mm according the simulated impedance bandwidth.

We also note the first resonant frequency of the sleeve monopole antenna, compared with the monopole antenna, slightly increases when introducing the parasitic radiators. When the parasitic arms present, the virtual feed point shifts to the open end side, leading to the decrease of the effective length of the monopole radiator.

B. CONVERGENCE EFFECT OF THE SPPs COMPOSITE METASURFACE

To demonstrate the effects of the metasurface on the antenna gain enhancement, the basic TSA (Ant. 1), the SPPs-loaded TSA (Ant. 2), and the composite metasurface loaded antenna (Ant. 3) are compared by simulations. The converging effect of the metasurface on EM wave is presented below.

Fig. 5(a) shows the basic TSA without any loading. Its structure parameters are presented in the Section II, part A. The TSA shows a wideband gain of 11 dBi from 21 GHz to 31 GHz (refer to Fig. 9(b)). Fig. 5(b) shows the SPPs loaded TSA, where the corrugated SPPs strip is made of cross-shaped unit cells arranged periodically on the upper surface of Substrate 2. The unit cell has a periodicity $p = 0.6$ mm and the trip width $a = p/2$. The groove height h determines the asymptotic frequency of the SPPs structure. Since the asymptotic frequency should be above the working frequency of the antenna (20-32 GHz), the groove height h is finally set as 0.85 mm according to the simulated dispersion diagram shown in Fig. 6(a). Here, only the odd modes are concerned because the electric fields of the interesting modes should be consistent with those in TSA's aperture [29], [31], [32].

The plasmonic structure is used to manipulate surface wave propagation and further to adjust the phase of the EM surface wave [29]. The fundamental is that the propagation

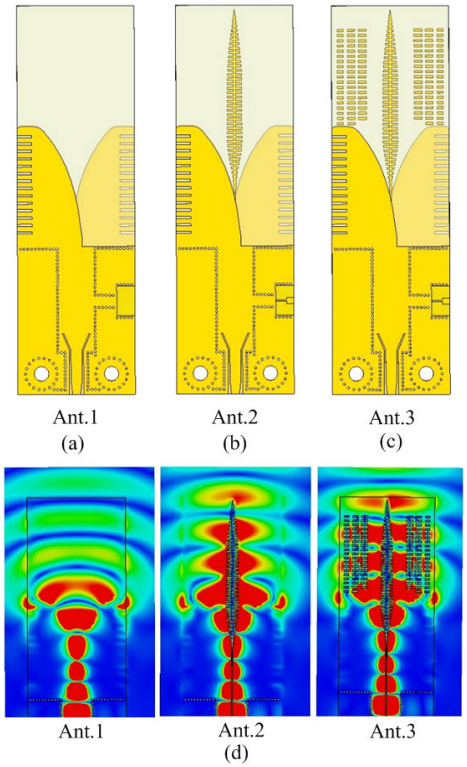

FIGURE 5. (a) The basic tapered slot antenna (TSA). (b) The SPPs-loaded TSA. (c) The composite metasurface loaded antenna. (d) Contour plots of electric field of three antennas at 26 GHz.

constant β_{SPP} can be engineered by varying the geometrical parameters of the unit cell. β_{SPP} is approximately presented as [33]

$$\beta_{SPP} = k_0\sqrt{1 + (a/p)^2 \tan^2(k_0 h)} \tag{1}$$

where k_0 is the wave number of the EM wave in free space. In a simple case where the spoof SPPs transmission line (TL) is surrounded by air, the propagation constant β_{SPP} will be larger than k_0, i.e. the EM field propagating along SPPs TL has a slower phase velocity than light speed in free space. For surface wave, the refractive index n_{SPP} seen by the wave can be given by the ratio of the speed of light in free space to the phase velocity of the wave along the surface [22]. Consequently, the equivalent refractive index n_{SPP} can be extracted from the simulated dispersion diagram by

$$n_{SPP} = \beta_{SPP}/k_0 \tag{2}$$

Therefore, the plasmonic structure can be equivalently taken as dielectric with a larger refractive index. The equivalent refractive index in the frequency range of interest is shown in Fig. 6(b). Two transition regions with gradually increased groove height are designed to achieve propagation constant match between TM mode in slot and SPPs mode [29], [34]–[36]. The total length of the SPPs structure (L_{SPP}) is finally determined by the operating frequency of the omnidirectional monopole antenna.

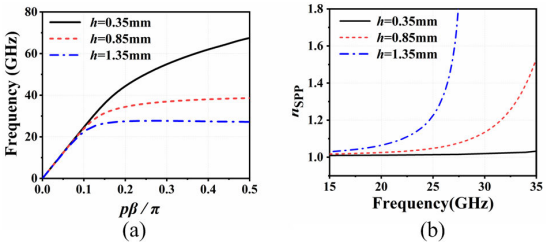

FIGURE 6. Influence of the groove depth of SPPs structure (h) on (a) the dispersion and (b) the effective refractive index (n_{SPP}).

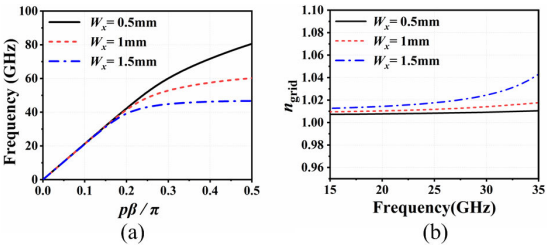

FIGURE 7. Influence of the lengths of grid array (W_x) on (a) the dispersion and (b) the effective refractive index (n_{grid}).

In Fig. 5(c), metal grid arrays are added on the antenna to form the composite metasurface to further enhance the converging effect. Metal grid arrays are often used to obtain inductive surface for the frequency selective surface (FSS), where the grids resonate and show a narrow frequency band [37]. To avoid resonance and obtain wideband operation, much shorter grids are adopted here. As shown in Fig. 7(a), while the grid length (W_x) increases from 0.5 mm to 1.5 mm, the EM wave propagating along the grid array shows a larger propagation constant and a lower asymptotic frequency as well. The method applied for SPPs structure is reused to extract the effective refractive index for the grid arrays. The effective refractive index n_{grid} is shown in Fig. 7(b), where the refractive index can be tuned by varying the grid length. By properly choosing structural parameters, the graded refractive indexes [22], [29], i.e. $n_{SPP} > n_{grid} > n_0$, can be obtained as shown in Fig. 8. We can equivalently consider the composite metasurface as a lens with refraction index grading along y direction in E-plane of the TSA [29]. When EM wave travels along the composite metasurface, its phase plane becomes flatter [38], [39]. By this means, narrow beam widths can be obtained. To validate the effect of the composite metasurface, full wave simulations were performed.

The simulated far field patterns in E-plane for these antennas are shown in Fig. 9(a). As expected, with the loading of the metasurface, the beam width of antennas becomes narrower. Fig. 9(b) shows the simulated gain of these antennas. Compared with the basic antenna (Ant. 1), Ant. 2 shows a 1.63 dBi gain enhancement. The gain is further enhanced to 13.09 dBi at 27.5 GHz for Ant. 3 by adding the grid arrays. An average gain enhancement of 2 dBi is achieved for Ant. 3 over the frequency range of 18-31 GHz. It is evident that

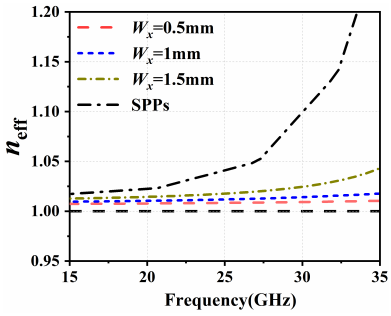

FIGURE 8. Effective refractive index (n_{eff}) distribution along the y direction: n_{SPP}, n_{grid} and n_0.

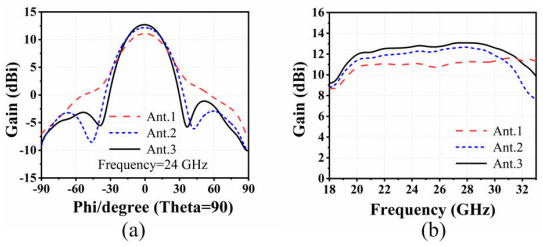

FIGURE 9. (a) Radiation performance of the proposed antenna (E-plane) at 24GHz. (b) Gain comparison chart of three antennas.

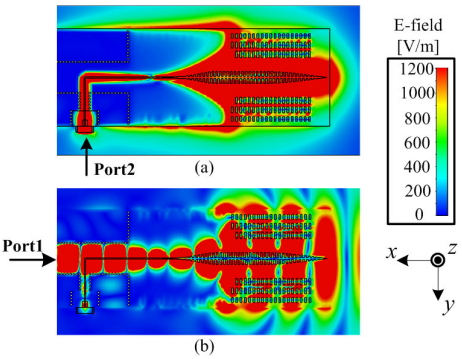

FIGURE 10. Simulated electric field of the antenna. (a) 2.48GHz, (b) 26GHz.

the composite metasurface can effectively narrow the beam width and thus improve the gain of the TSA.

C. THE FEEDING SCHEME AND THE ISOLATION

To obtain a high isolation, the endfire antenna is fed through the SIW and omnidirectional antenna through the integrated coaxial line. It is well known that the SIW cannot support TEM waves. The TEM mode traveling along the integrated coaxial line cannot reach Port 1 as shown in Fig. 10(a). Thus a high isolation ($|S_{12}| < -35$ dB) is achieved between Port 2 and Port 1. However, the EM energy may leak into the integrated coaxial line when it is input from Port 1 through the SIW. The leakage energy can be safely reduced when the cutoff frequency of the integrated coaxial line for TE mode is higher than the operating frequency (K/Ka-band). The high cutoff frequency can be achieved by narrowing the width of sleeve of the integrated coaxial line. Through simulation, the width of $L_d = 2.16$ mm is chosen to suppress EM wave

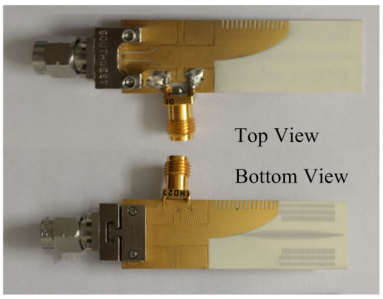

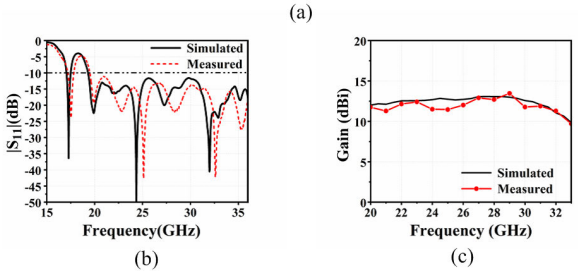

FIGURE 11. (a) Photograph of the antenna prototype. (b) Measured and simulated reflection coefficients $|S_{11}|$. (c) Measured and simulated gain.

from Port 1 to Port 2. The $|S_{21}|$ is below -25 dB, indicating a good isolation. Fig. 10(b) shows the contour plot of electric field when Port 1 is fed.

III. EXPERIMENTAL RESULTS AND DISCUSSION

A prototype of the proposed antenna is fabricated as shown in Fig. 11(a), and validated experimentally. For the MMW endfire antenna, the measured results are shown in Fig. 11(b) and (c). The reflection coefficient ($|S_{11}|$), shown in Fig. 11(b), exhibits a large operating BW. The 3 dB gain BW_2 is the range of 19.32-32.9 GHz (52%) with a peak gain of 13.09 dBi, which is consistent with simulated results, as shown in Fig. 11(c). The radiation pattern of the endfire antenna is also measured in both the E- (x-y plane) and H-planes (x-z plane) at 20 GHz, 24 GHz, 26 GHz, and 30 GHz, as shown in Fig. 12. All measured radiation patterns remain stable in endfire direction and agree quite well with the prediction from simulations. Compared with [29], a little lower endfire gain obtained is mainly due to the shorter SPPs-structure.

Figs. 13(a) and (b) show the simulated and measured results of the omnidirectional planar open sleeve monopole antenna. The measured results indicate impedance BW_1 ($|S_{11}| < -10$ dB) of 49.3% from 2.23 GHz to the frequency 3.69 GHz. The gain is around 2 dB in operating band and the peak gain is measured at 3.58 GHz. The far-field patterns in the E- and H-plane at 2.48 GHz, and 3.38 GHz are shown in Fig. 14. An omnidirectional radiation pattern is observed. The slight discrepancy of the radiation patterns between measured and simulated ones is owing to the asymmetric structure of the antenna caused by Port 2.

The isolation between the two antennas is measured and shown in the Fig. 15. While Port 1 is under test, Port 2 is loaded with a standard 50 Ω load, and vice versa. At the

TABLE 1. Performance comparison with the previous structure-shared large frequency ratio antennas.

Ref.	f_{01}, f_{02} (GHz)	f_{02}/f_{01} (frequency ratio)	BW_1, BW_2	Peak gain (dBi)	Antenna electrical size ($\lambda_0\times\lambda_0\times\lambda_0$) @ f_{01}	Shared elements
[9]	0.9,2.5	2.8	26.6%, 42.2%	8. 4, 8	0.72×0.37×0.14	N.A.
[13]	2.4, 24	10	38.24%, 16.18%	7, 11.3	1.2×1.2×0.304	3-D DR
[14]	2.4, 24	10	30.77%, 4.67%	6.8, 18.2	0.8×0.8×0.19	3-D hollow DR
[15]	3.5, 60	17	2.6%, 2.4%	7.3, 24	0.42×0.30×0.02	SIW cavity
[40]	0.4,15	37.5	24.0%, 12.7%	7.5, 23.4	0.40×0.40×0.10	N.A.
This work	2.4, 26	10.8	**49.3%, 52%**	2.91, 13.09	0.42×0.13×**0.004**	SPPs

λ_0 is the free-space wavelength at f_{01}, and f_{01} (f_{02}) is the low (high) band center frequency.

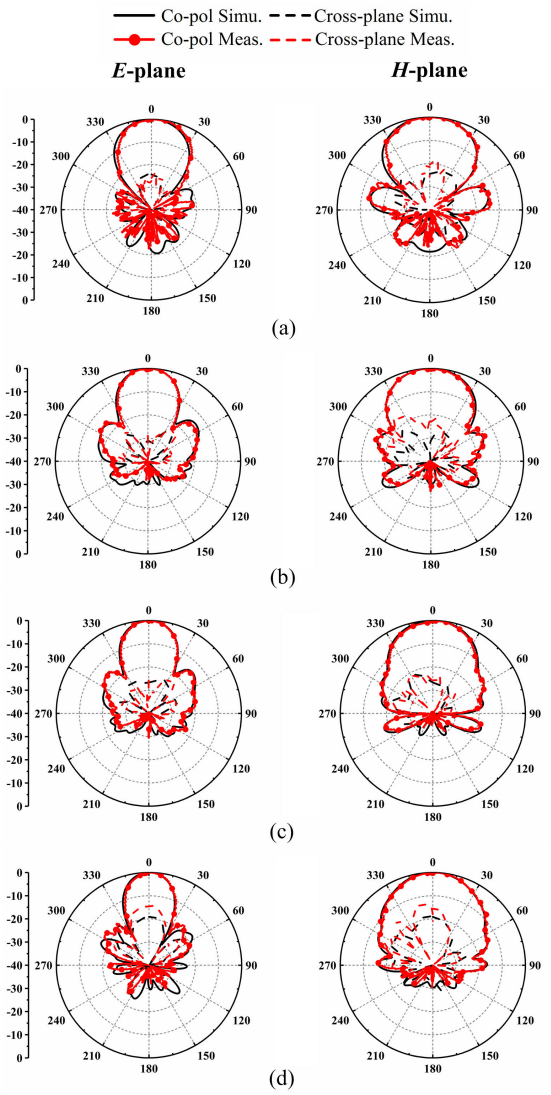

FIGURE 12. Measured and simulated radiation patterns of the proposed antenna. (a)–(d) E-plane and H-plane patterns at 20, 24, 26, and 30 GHz.

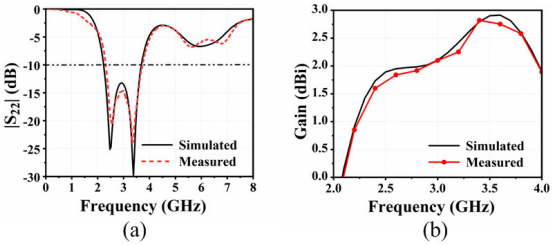

FIGURE 13. (a) Measured and simulated reflection coefficients $|S_{22}|$. (b) Measured and simulated gain.

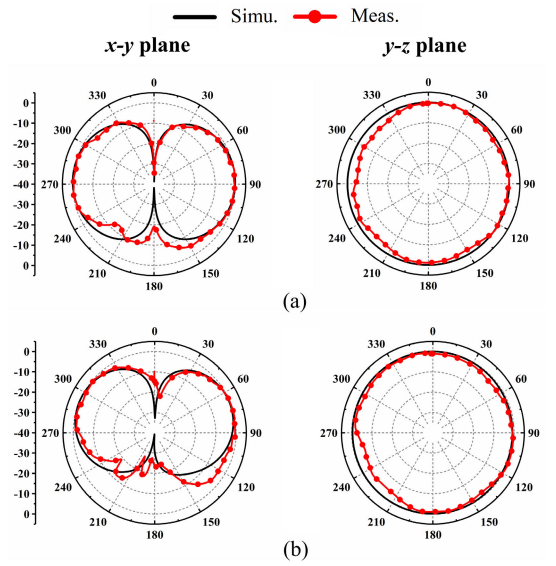

FIGURE 14. Measured and simulated radiation patterns of the proposed antenna. (a) x-y plane and y-z plane at 2.48 GHz. (b) x-y plane and y-z plane at 3.38 GHz.

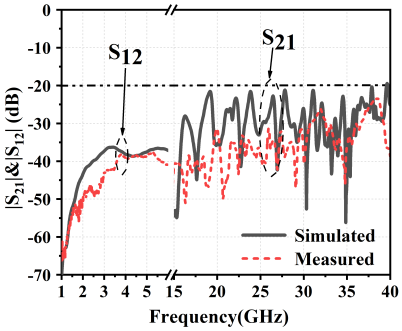

FIGURE 15. The isolation of the proposed antenna.

microwave band, the isolation is as high as 35 dB, and at the MMW band, larger than 25 dB, which shows a good isolation and further verifies the isolation scheme presented in Section II, part D.

A comparison between the proposed antenna and other reference antennas is given in Table 1. The proposed antenna shows a much lower profile than the DRAs in [13], [14], while keeping a wide operating bandwidth [15].

IV. CONCLUSION

In this paper, an SPPs-shared technique is proposed to construct the dual band antenna operating at both 2.23-3.69 GHz (S-band) and 19.32-32.90 GHz (K/Ka-band). The SPPs structure functions as a planar open sleeve monopole at S-band, while as a metasurface for endfire antenna at K/Ka-band. The antenna is fabricated on a dual-layer PCB, showing a compact size and a low profile. Simulated and measured results indicate that the antenna has a broad BW 49.3% and a high realized gain 2.92 dBi for the S-band, and 52% and 13.09 dBi for the K/Ka-band. It would be attractive for the applications of future wireless communication systems.

REFERENCES

[1] D. Li, Z. Shen, and E.-P. Li, "Spurious-free dual-band bandpass frequency-selective surfaces with large band ratio," *IEEE Trans. Antennas Propag.*, vol. 67, no. 2, pp. 1065–1072, Feb. 2019.
[2] L. Y. Feng and K. W. Leung, "Dual-frequency folded-parallel-plate antenna with large frequency ratio," *IEEE Trans. Antennas Propag.*, vol. 64, no. 1, pp. 340–345, Jan. 2016.
[3] D. Wang and C. H. Chan, "Multiband antenna for WiFi and WiGig communications," *IEEE Antennas Wireless Propag. Lett.*, vol. 15, pp. 309–312, 2016.
[4] A. Boukarkar, X. Q. Lin, Y. Jiang, and Y. Q. Yu, "Miniaturized single-feed multiband patch antennas," *IEEE Trans. Antennas Propag.*, vol. 65, no. 2, pp. 850–854, Feb. 2017.
[5] H. S. Gusain, S. Raghavan, and P. H. Rao, "Shared aperture printed slot antenna," in *Proc. 3rd Int. Conf. Comput., Commun. Netw. Technol. (ICCCNT*, Coimbatore, India, Jul. 2012, pp. 1–4.
[6] T. Zhihong, Y. P. Zhang, C. Luxey, A. Bisognin, D. Titz, and F. Ferrero, "A Ceramic antenna for tri-band radio devices," *IEEE Trans. Antennas Propag.*, vol. 61, no. 11, pp. 5776–5780, Nov. 2013.
[7] L. Zhang, K. Y. See, B. Zhang, and Y. P. Zhang, "Integration of dual-band monopole and microstrip grid array for single-chip tri-band application," *IEEE Trans. Antennas Propag.*, vol. 61, no. 1, pp. 439–443, Jan. 2013.
[8] C. Han, C. Rodenbeck, J. Huang, and K. Chang, "A C/Ka dual frequency dual layer circularly polarized reflectarray antenna with microstrip ring elements," *IEEE Trans. Antennas Propag.*, vol. 52, no. 11, pp. 2871–2876, Nov. 2004.
[9] P. Li, K. Luk, and K. Lau, "A dual-feed dual-band L-probe patch antenna," *IEEE Trans. Antennas Propag.*, vol. 53, no. 7, pp. 2321–2323, Jul. 2005.
[10] L. Y. Nie, X. Q. Lin, Z. Q. Yang, J. Zhang, and B. Wang, "Structure-shared planar UWB MIMO antenna with high isolation for mobile platform," *IEEE Trans. Antennas Propag.*, vol. 67, no. 4, pp. 2735–2738, Apr. 2019.
[11] L.-H. Wen, S. Gao, Q. Luo, C.-X. Mao, W. Hu, Y. Yin, Y. Zhou, and Q. Wang, "Compact dual-polarized shared-dipole antennas for base station applications," *IEEE Trans. Antennas Propag.*, vol. 66, no. 12, pp. 6826–6834, Dec. 2018.
[12] K. Wang, X. Liang, W. Zhu, J. Geng, J. Li, Z. Ding, and R. Jin, "A dual-wideband dual-polarized aperture-shared patch antenna with high isolation," *IEEE Antennas Wireless Propag. Lett.*, vol. 17, no. 5, pp. 735–738, May 2018.
[13] L. Y. Feng and K. W. Leung, "Wideband dual-frequency antenna with large frequency ratio," *IEEE Trans. Antennas Propag.*, vol. 67, no. 3, pp. 1981–1986, Mar. 2019.
[14] L. Y. Feng and K. W. Leung, "Dual-fed hollow dielectric antenna for dual-frequency operation with large frequency ratio," *IEEE Trans. Antennas Propag.*, vol. 65, no. 6, pp. 3308–3313, Jun. 2017.
[15] J. F. Zhang, Y. J. Cheng, Y. R. Ding, and C. X. Bai, "A dual-band shared-aperture antenna with large frequency ratio, high aperture reuse efficiency, and high channel isolation," *IEEE Trans. Antennas Propag.*, vol. 67, no. 2, pp. 853–860, Feb. 2019.
[16] A. Osseiran, J. F. Monserrat, and P. Marsch, *5G Mobile and Wireless Communications Technology*. Cambridge, U.K.: Cambridge Univ. Press, 2016.
[17] R. Lian, Z. Wang, Y. Yin, J. Wu, and X. Song, "Design of a low-profile dual-polarized stepped slot antenna array for base station," *IEEE Antennas Wireless Propag. Lett.*, vol. 15, pp. 362–365, 2016.
[18] G. C. Huang, M. F. Iskander, M. Hoque, S. R. Goodall, and T. Bocskor, "Antenna array design and system for directional networking," *IEEE Antennas Wireless Propag. Lett.*, vol. 14, pp. 1141–1144, 2015.
[19] P. Liu, X. Zhu, Z. H. Jiang, Y. Zhang, H. Tang, and W. Hong, "A compact single-layer q-band tapered slot antenna array with phase-shifting inductive windows for endfire patterns," *IEEE Trans. Antennas Propag.*, vol. 67, no. 1, pp. 169–178, Jan. 2019.
[20] A. O. Diallo, R. Czarny, B. Loiseaux, and S. Hole, "Comparison between a thin lens antenna made of structured dielectric material and conventional lens antennas, in Q-band in a compact volume," *IEEE Antennas Wireless Propag. Lett.*, vol. 17, no. 2, pp. 307–310, Feb. 2018.
[21] I. Kadri, A. Petosa, and L. Roy, "Ka-band Fresnel lens antenna fed with an active linear microstrip patch array," *IEEE Trans. Antennas Propag.*, vol. 53, no. 12, pp. 4175–4178, Dec. 2005.
[22] B. H. Fong, J. S. Colburn, J. J. Ottusch, J. L. Visher, and D. F. Sievenpiper, "Scalar and tensor holographic artificial impedance surfaces," *IEEE Trans. Antennas Propag.*, vol. 58, no. 10, pp. 3212–3221, Oct. 2010.
[23] X. Wang, Z. Li, X. Fei, and J. Wang, "A holographic antenna based on spoof surface plasmon polaritons," *IEEE Antennas Wireless Propag. Lett.*, vol. 17, no. 8, pp. 1528–1532, Aug. 2018.
[24] A. Dadgarpour, B. Zarghooni, B. S. Virdee, and T. A. Denidni, "Improvement of gain and elevation tilt angle using metamaterial loading for millimeter-wave applications," *IEEE Antennas Wireless Propag. Lett.*, vol. 15, pp. 418–420, 2016.
[25] E. Erfani, M. Niroo-Jazi, and S. Tatu, "A high-gain broadband gradient refractive index metasurface lens antenna," *IEEE Trans. Antennas Propag.*, vol. 64, no. 5, pp. 1968–1973, May 2016.
[26] Y. Shi, K. Li, J. Wang, L. Li, and C.-H. Liang, "An etched planar metasurface half maxwell fish-eye lens antenna," *IEEE Trans. Antennas Propag.*, vol. 63, no. 8, pp. 3742–3747, Aug. 2015.
[27] T. Hongnara, S. Chaimool, P. Akkaraekthalin, and Y. Zhao, "Design of compact beam-steering antennas using a metasurface formed by uniform square rings," *IEEE Access*, vol. 6, pp. 9420–9429, 2018.
[28] A. K. Singh, M. P. Abegaonkar, and S. K. Koul, "High-gain and high-aperture-efficiency cavity resonator antenna using metamaterial superstrate," *IEEE Antennas Wireless Propag. Lett.*, vol. 16, pp. 2388–2391, 2017.
[29] X.-F. Zhang, W.-J. Sun, and J.-X. Chen, "Millimeter-wave ATS antenna with wideband-enhanced endfire gain based on coplanar plasmonic structures," *IEEE Antennas Wireless Propag. Lett.*, vol. 18, no. 5, pp. 826–830, May 2019.
[30] W. Tan and Z. Shen, "A dual-band dual-sleeve monopole antenna," *IEEE Antennas Wireless Propag. Lett.*, vol. 16, pp. 2951–2954, 2017.
[31] Y. Han, S. Gong, J. Wang, Y. Li, Y. Fan, J. Zhang, and S. Qu, "Shared-aperture antennas based on even-and odd-mode spoof surface plasmon polaritons," *IEEE Trans. Antennas Propag.*, to be published, doi: 10.1109/tap.2019.2944548.
[32] X. Du, H. Li, and Y. Yin, "Wideband fish-bone antenna utilizing odd-mode spoof surface plasmon polaritons for end-fire radiation," *IEEE Trans. Antennas Propag.*, vol. 67, no. 7, pp. 4848–4853, Jul. 2019.
[33] H. F. Ma, X. Shen, Q. Cheng, W. X. Jiang, and T. J. Cui, "Broadband and high-efficiency conversion from guided waves to spoof surface plasmon polaritons," *Laser Photon. Rev.*, vol. 8, no. 1, pp. 146–151, Jan. 2014.
[34] A. Kandwal, Q. Zhang, X. Tang, L. W. Liu, and G. Zhang, "Low-profile spoof surface plasmon polaritons traveling-wave antenna for near-endfire radiation," *IEEE Antennas Wireless Propag. Lett.*, vol. 17, no. 2, pp. 184–187, Feb. 2018.
[35] Z.-B. Yang, D.-F. Guan, Q. Zhang, P. You, X. Huang, X.-X. Hou, S.-D. Xu, and S.-W. Yong, "Low-loss spoof surface plasmon polariton based on folded substrate integrated waveguide," *IEEE Antennas Wireless Propag. Lett.*, vol. 18, no. 1, pp. 222–225, Jan. 2019.
[36] J. J. Xu, H. C. Zhang, Q. Zhang, and T. J. Cui, "Efficient conversion of surface-plasmon-like modes to spatial radiated modes," *Appl. Phys. Lett.*, vol. 106, no. 2, Jan. 2015, Art. no. 021102.
[37] D. Ferreira, I. Cuinas, R. F. S. Caldeirinha, and T. R. Fernandes, "3-D mechanically tunable square slot FSS," *IEEE Trans. Antennas Propag.*, vol. 65, no. 1, pp. 242–250, Jan. 2017.
[38] J.-L. Liu, T. Su, and Z.-X. Liu, "High-gain grating antenna with surface wave launcher array," *IEEE Antennas Wireless Propag. Lett.*, vol. 17, no. 4, pp. 706–709, Apr. 2018.
[39] S. Zhu, H. Liu, and P. Wen, "A new method for achieving miniaturization and gain enhancement of Vivaldi antenna array based on anisotropic metasurface," *IEEE Trans. Antennas Propag.*, vol. 67, no. 3, pp. 1952–1956, Mar. 2019.

[40] S.-G. Zhou, P.-K. Tan, and T.-H. Chio, "Wideband, low profile P- and Ku-band shared aperture antenna with high isolation and low cross-polarisation," *IET Microw., Antennas Propag.*, vol. 7, no. 4, pp. 223–229, Mar. 2013.

JIAN-XIN CHEN (Senior Member, IEEE) was born in Nantong, Jiangsu, China, in 1979. He received the B.S. degree from the Huai Yin Teachers College, Jiangsu, China, in 2001, the M.S. degree from the University of Electronic Science and Technology of China (UESTC), Chengdu, China, in 2004, and the Ph.D. degree from the City University of Hong Kong, Hong Kong, in 2008.

Since 2009, he has been with Nantong University, Jiangsu, where he is currently a Professor. He has authored or coauthored more than 80 internationally refereed journal articles and conference papers. He holds three Chinese patents and two U.S. patents. His research interests include microwave active/passive circuits and antennas, LTCC-based millimeter-wave circuits, and antennas. He was a recipient of the Best Paper Award presented at the Chinese National Microwave and Millimeter-Wave Symposium, Ningbo, China, in 2007. He was Supervisor of 2014 iWEM student innovation competition winner in Sapporo, Japan.

SHUAI-HUA CAO was born in Nantong, Jiangsu, China, in 1996. He received the B.Sc. degree in communication engineering from Nantong University, Nantong, China, in 2018. He is currently pursuing the M.Sc. degree in electromagnetic field and microwave technology with Nantong University, Nantong. His current research interest includes antenna.

XUE-FENG ZHANG was born in Zaoyang, Hubei, China, in 1975. He received the B.S. degree from Huibei University, China, in 1998, and the M.S. and Ph.D. degrees from the Huazhong University of Science and Technology (HUST), Wuhan, China, in 2004 and 2008, respectively. Since 2008, he has been with Nantong University, Jiangsu, China. His current research interests include metamaterial-based millimeter-wave circuits and antennas, and novel semiconductor devices.